Biomedical Optics EXPRESS

Deep-UV biological imaging by lanthanide ion molecular protection

Yasuaki Kumamoto,[1,2,4] Katsumasa Fujita,[1] Nicholas Isaac Smith,[3] and Satoshi Kawata[1,2,*]

[1]*Department of Applied Physics, Osaka University, 2-1 Yamadaoka, Suita, Osaka 565-0871, Japan*
[2]*Near-field Nanophotonics Research Team, RIKEN, 2-1 Hirosawa, Wako, Saitama 351-0198, Japan*
[3]*Immunology Frontier Research Center, Osaka University, 3-1 Yamadaoka, Suita, Osaka 565-0871, Japan*
[4]*Currently with the Department of Pathology and Cell Regulation, Kyoto Prefectural University of Medicine, 465 Kajii-cho Kawaramachi-Hirokoji, Kamigyo-ku, Kyoto 602-8566, Japan*
[*]*kawata@ap.eng.osaka-u.ac.jp*

Abstract: Deep-UV (DUV) light is a sensitive probe for biological molecules such as nucleobases and aromatic amino acids due to specific absorption. However, the use of DUV light for imaging is limited because DUV can destroy or denature target molecules in a sample. Here we show that trivalent ions in the lanthanide group can suppress molecular photodegradation under DUV exposure, enabling a high signal-to-noise ratio and repetitive DUV imaging of nucleobases in cells. Underlying mechanisms of the photodegradation suppression can be excitation relaxation of the DUV-absorptive molecules due to energy transfer to the lanthanide ions, and/or avoiding ionization and reactions with surrounding molecules, including generation of reactive oxygen species, which can modify molecules that are otherwise transparent to DUV light. This approach, directly removing excited energy at the fundamental origin of cellular photodegradation, indicates an important first step towards the practical use of DUV imaging in a variety of biological applications.

OCIS codes: (300.6540) Spectroscopy, ultraviolet; (170.3880) Medical and biological imaging; (260.5130) Photochemistry.

References and links

1. Commercially available from Shimadzu, Inc, JASCO, Inc, etc.
2. Commercially available from Nikkiso, Inc.
3. S. Song and S. A. Asher, "UV resonance Raman studies of peptide conformation in poly(L-lysine), poly(L-glutamic acid), and model complexes: the basis for protein secondary structure determinations," J. Am. Chem. Soc. **111**(12), 4295–4305 (1989).
4. K. R. Rodgers, C. Su, S. Subramaniam, and T. G. Spiro, "Hemoglobin R→T structural dynamics from simultaneous monitoring of tyrosine and tryptophan time-resolved UV resonance Raman signals," J. Am. Chem. Soc. **114**(10), 3697–3709 (1992).
5. Z. Chi and S. A. Asher, "UV resonance Raman determination of protein acid denaturation: selective unfolding of helical segments of horse myoglobin," Biochemistry **37**(9), 2865–2872 (1998).
6. S. Nagatomo, M. Nagai, Y. Mizutani, T. Yonetani, and T. Kitagawa, "Quaternary structures of intermediately ligated human hemoglobin A and influences from strong allosteric effectors: resonance Raman investigation," Biophys. J. **89**(2), 1203–1213 (2005).
7. S. F. El-Mashtoly, H. Takahashi, T. Shimizu, and T. Kitagawa, "Ultraviolet resonance Raman evidence for utilization of the heme 6-propionate hydrogen-bond network in signal transmission from heme to protein in Ec DOS protein," J. Am. Chem. Soc. **129**(12), 3556–3563 (2007).
8. G. Balakrishnan, C. L. Weeks, M. Ibrahim, A. V. Soldatova, and T. G. Spiro, "Protein dynamics from time resolved UV Raman spectroscopy," Curr. Opin. Struct. Biol. **18**(5), 623–629 (2008).
9. C. Wei, G. Jia, J. Yuan, Z. Feng, and C. Li, "A spectroscopic study on the interactions of porphyrin with G-quadruplex DNAs," Biochemistry **45**(21), 6681–6691 (2006).
10. S. P. A. Fodor, R. P. Rava, T. R. Hays, and T. G. Spiro, "Ultraviolet resonance Raman spectroscopy of the nucleotides with 266-, 240-, 218-, and 200-nm pulsed laser excitation," J. Am. Chem. Soc. **107**(6), 1520–1529 (1985).
11. C. R. Johnson, M. Ludwig, and S. A. Asher, "Ultraviolet resonance Raman characterization of photochemical transients of phenol, tyrosine, and tryptophan," J. Am. Chem. Soc. **108**(5), 905–912 (1986).

#253648 Received 9 Nov 2015; revised 8 Dec 2015; accepted 11 Dec 2015; published 18 Dec 2015

12. D. N. Nikogosyan and H. Görner, "Photolysis of aromatic amino acids in aqueous solution by nanosecond 248 and 193 nm laser light," J. Photochem. Photobiol. B **13**(3-4), 219–234 (1992).
13. H. Görner, "Photochemistry of DNA and related biomolecules: quantum yields and consequences of photoionization," J. Photochem. Photobiol. B **26**(2), 117–139 (1994).
14. K. Lao and A. N. Glazer, "Ultraviolet-B photodestruction of a light-harvesting complex," Proc. Natl. Acad. Sci. U.S.A. **93**(11), 5258–5263 (1996).
15. C. E. Crespo-Hernández, S. Flores, C. Torres, I. Negrón-Encarnación, and R. Arce, "Photochemical and photophysical studies of guanine derivatives: intermediates contributing to its photodestruction mechanism in aqueous solution and the participation of the electron adduct," Photochem. Photobiol. **71**(5), 534–543 (2000).
16. Q. Wu, G. Balakrishnan, A. Pevsner, and T. G. Spiro, "Histidine photodegradation during UV resonance Raman spectroscopy," J. Phys. Chem. A **107**(40), 8047–8051 (2003).
17. M. Harz, R. A. Claus, C. L. Bockmeyer, M. Baum, P. Rösch, K. Kentouche, H.-P. Deigner, and J. Popp, "UV-resonance Raman spectroscopic study of human plasma of healthy donors and patients with thrombotic microangiopathy," Biopolymers **82**(4), 317–324 (2006).
18. D. I. Pattison and M. J. Davies, "Actions of ultraviolet light on cellular structures," in *Cancer: Cell structures, carcinogens and genomic instability*, L. P. Bignold, ed. (Birkhaeuser, 2006).
19. Y. Kumamoto, A. Taguchi, N. I. Smith, and S. Kawata, "Deep UV resonant Raman spectroscopy for photodamage characterization in cells," Biomed. Opt. Express **2**(4), 927–936 (2011).
20. J.-L. Ravanat, T. Douki, and J. Cadet, "Direct and indirect effects of UV radiation on DNA and its components," J. Photochem. Photobiol. B **63**(1-3), 88–102 (2001).
21. C. T. Middleton, K. de La Harpe, C. Su, Y. K. Law, C. E. Crespo-Hernández, and B. Kohler, "DNA excited-state dynamics: from single bases to the double helix," Annu. Rev. Phys. Chem. **60**(1), 217–239 (2009).
22. B. J. Zeskind, C. D. Jordan, W. Timp, L. Trapani, G. Waller, V. Horodincu, D. J. Ehrlich, and P. Matsudaira, "Nucleic acid and protein mass mapping by live-cell deep-ultraviolet microscopy," Nat. Methods **4**(7), 567–569 (2007).
23. M. C. Cheung, J. G. Evans, B. McKenna, and D. J. Ehrlich, "Deep ultraviolet mapping of intracellular protein and nucleic acid in femtograms per pixel," Cytometry A **79**(11), 920–932 (2011).
24. M. C. Cheung, R. LaCroix, B. K. McKenna, L. Liu, J. Winkelman, and D. J. Ehrlich, "Intracellular protein and nucleic acid measured in eight cell types using deep-ultraviolet mass mapping," Cytometry A **83**(6), 540–551 (2013).
25. Y. Kumamoto, A. Taguchi, N. I. Smith, and S. Kawata, "Deep ultraviolet resonant Raman imaging of a cell," J. Biomed. Opt. **17**(7), 076001 (2012).
26. B. Banerjee, T. Renkoski, L. R. Graves, N. S. Rial, V. L. Tsikitis, V. Nfonsam, J. Pugh, P. Tiwari, H. Gavini, and U. Utzinger, "Tryptophan autofluorescence imaging of neoplasms of the human colon," J. Biomed. Opt. **17**(1), 016003 (2012).
27. S. Pallu, G. Y. Rochefort, C. Jaffre, M. Refregiers, D. B. Maurel, D. Benaitreau, E. Lespessailles, F. Jamme, C. Chappard, and C. L. Benhamou, "Synchrotron ultraviolet microspectroscopy on rat cortical bone: involvement of tyrosine and tryptophan in the osteocyte and its environment," PLoS One **7**(8), e43930 (2012).
28. F. Jamme, S. Kascakova, S. Villette, F. Allouche, S. Pallu, V. Rouam, and M. Réfrégiers, "Deep UV autofluorescence microscopy for cell biology and tissue histology," Biol. Cell **105**(7), 277–288 (2013).
29. M. Kikawada, A. Ono, W. Inami, and Y. Kawata, "Enhanced multicolor fluorescence in bioimaging using deep-ultraviolet surface plasmon resonance," Appl. Phys. Lett. **104**(22), 223703 (2014).
30. M. Kikawada, A. Ono, W. Inami, and Y. Kawata, "Surface plasmon-enhanced fluorescence cell imaging in deep-UV region," Appl. Phys. Express **8**(7), 072401 (2015).
31. D.-K. Yao, K. Maslov, K. K. Shung, Q. Zhou, and L. V. Wang, "In vivo label-free photoacoustic microscopy of cell nuclei by excitation of DNA and RNA," Opt. Lett. **35**(24), 4139–4141 (2010).
32. D.-K. Yao, R. Chen, K. Maslov, Q. Zhou, and L. V. Wang, "Optimal ultraviolet wavelength for *in vivo* photoacoustic imaging of cell nuclei," J. Biomed. Opt. **17**(5), 056004 (2012).
33. A. Jirasek, H. Georg Schulze, C. H. Hughesman, A. Louise Creagh, C. A. Haynes, M. W. Blades, and R. F. B. Turner, "Discrimination between UV radiation-induced and thermally induced spectral changes in AT-paired DNA oligomers using UV resonance Raman spectroscopy," J. Raman Spectrosc. **37**(12), 1368–1380 (2006).
34. S. Chadha, W. H. Nelson, and J. F. Sperry, "Ultraviolet micro-Raman spectrograph for the detection of small numbers of bacterial cells," Rev. Sci. Instrum. **64**(11), 3088–3093 (1993).
35. F. S. Richardson, "Terbium(III) and europium(III) ions as luminescent probes and stains for biomolecular systems," Chem. Rev. **82**(5), 541–552 (1982).
36. A. A. Lamola and J. Eisinger, "Excited states of nucleotides in water at room temperature," Biochim. Biophys. Acta **240**(3), 313–325 (1971).
37. M. D. Topal and J. R. Fresco, "Fluorescence of terbium ion-nucleic acid complexes: a sensitive specific probe for unpaired residues in nucleic acids," Biochemistry **19**(24), 5531–5537 (1980).
38. M. S. Kayne and M. Cohn, "Enhancement of Tb(III) and Eu(III) fluorescence in complexes with Escherichia coli tRNA," Biochemistry **13**(20), 4159–4165 (1974).
39. Z. Balcarová and V. Brabec, "Reinterpretation of fluorescence of terbium ion-DNA complexes," Biophys. Chem. **33**(1), 55–61 (1989).
40. J. Eisinger and A. A. Lamola, "Europium ions as probes for excited molecules in aqueous solution," Biochim. Biophys. Acta **240**(3), 299–312 (1971).
41. W. D. Horrocks, Jr. and W. E. Collier, "Lanthanide ion luminescence probes. Measurement of distance between intrinsic protein fluorophores and bound metal ions: quantitation of energy transfer between tryptophan and

#253648 Received 9 Nov 2015; revised 8 Dec 2015; accepted 11 Dec 2015; published 18 Dec 2015

terbium(III) or europium (III) in the calcium-binding protein parvalbumin," J. Am. Chem. Soc. **103**(10), 2856–2862 (1981).
42. H. Niioka, T. Furukawa, M. Ichimiya, M. Ashida, T. Araki, and M. Hashimoto, "Multicolor cathodoluminescence microscopy for biological imaging with nanophosphors," Appl. Phys. Express **4**(11), 112402 (2011).
43. Cl^- was also added to the cells when Tb^{3+}, Eu^{3+}, or Tm^{3+} was added, but the amount of added Cl^- was only 2% of the total Cl^- existing in the buffer solution.
44. B. Rappaz, A. Barbul, Y. Emery, R. Korenstein, C. Depeursinge, P. J. Magistretti, and P. Marquet, "Comparative study of human erythrocytes by digital holographic microscopy, confocal microscopy, and impedance volume analyzer," Cytometry A **73**(10), 895–903 (2008).
45. Z. Q. Wen and G. J. Thomas, Jr., "UV resonance Raman spectroscopy of DNA and protein constituents of viruses: assignments and cross sections for excitations at 257, 244, 238, and 229 nm," Biopolymers **45**(3), 247–256 (1998).
46. R. H. Bisby, C. G. Morgan, I. Hamblett, and A. A. Gorman, "Quenching of singlet oxygen by Trolox C, ascorbate, and amino acids: effects of pH and temperature," J. Phys. Chem. A **103**(37), 7454–7459 (1999).
47. D. V. Bent and E. Hayon, "Excited state chemistry of aromatic amino acids and related peptides. I. Tyrosine," J. Am. Chem. Soc. **97**(10), 2599–2606 (1975).
48. D. V. Bent and E. Hayon, "Excited state chemistry of aromatic amino acids and related peptides. II. Phenylalanine," J. Am. Chem. Soc. **97**(10), 2606–2612 (1975).
49. D. V. Bent and E. Hayon, "Excited state chemistry of aromatic amino acids and related peptides. III. Tryptophan," J. Am. Chem. Soc. **97**(10), 2612–2619 (1975).
50. J. R. Lakowicz, "Energy transfer to multiple acceptors in one, two, or three dimensions," in *Principles of Fluorescence Spectroscopy*, J. R. Lakowicz, ed. (Springer, 2006).
51. Q. Zheng, S. Jockusch, Z. Zhou, and S. C. Blanchard, "The contribution of reactive oxygen species to the photobleaching of organic fluorophores," Photochem. Photobiol. **90**(2), 448–454 (2014).

1. Introduction

Deep-UV (DUV) light, corresponding to a wavelength range of 200-300 nm, is a sensitive probe of biological molecules which absorb DUV light remarkably well, but do not interact significantly with visible light, such as nucleobases, aromatic amino acids, and dopamine. DUV light has been used for label-free biomolecular detection in chromatography [1] and medical dialysis [2]. It has also been employed for precise analysis of local structures of macromolecules, such as proteins [3–8] and nucleic acids [9], by DUV spectroscopy. However, the practical use of DUV light for molecular imaging is limited. DUV light can destroy or denature biological molecules due to absorption [10–21], which restricts its use in quantitative, repetitive, and/or high signal-to-noise ratio (SNR) analyses of target molecules in a limited detection volume by DUV imaging, especially for samples involving trace amounts. Although a variety of advanced DUV imaging techniques measuring absorption [22–24], resonance Raman scattering [25], fluorescence [26–30], and photoacoustic signals [31,32] of DUV-absorptive molecules have been developed recently, the destructive nature of DUV light limits some unique benefits of these techniques in exploiting biological molecules, which could be measured with high sensitivity if the photodegradation could be avoided.

Suppressing the molecular photodegradation is essential for unlocking these limitations in the practical use of DUV light for biological imaging. Reducing the irradiation intensity in order to slowly accumulate signal is of little benefit because single photons can cause molecular photodegradation of nucleic acids and proteins under DUV exposure [12,13,17–21]. One part of the mechanisms of the molecular photodegradation under DUV exposure is related to how excited molecules react with oxygen (O_2) [12,13,18]. Generation of reactive oxygen species (ROS) occurs when O_2 accepts the excited molecular energy [12,13,18], which is demonstrated by removing O_2 from the environment, which then suppresses the molecular photodegradation under DUV exposure [12,13]. Additionally, since sample heating under DUV exposure can occur [33], cooling of the sample can also be a potential approach for suppressing the molecular photodegradation under DUV exposure, and has been demonstrated in some DUV Raman spectrograph setups [34]. However, these techniques can suppress only oxidation- or heat-based molecular degradation pathways but cannot protect molecules from the more direct ionization and dimerization that can occur after excitation by DUV light. They can be thought of secondary protective mechanisms, by removing the heat or secondary reactions that occur after photoexcitation. A more direct approach to quenching

#253648 Received 9 Nov 2015; revised 8 Dec 2015; accepted 11 Dec 2015; published 18 Dec 2015

or removing the energy from the system before it has passed to other molecules or dissipated as heat has the potential to offer a greater protective effect.

Here we report suppression of the molecular photodegradation under DUV exposure, and thereby demonstrate high SNR and repeatable DUV imaging of nucleobases in fixed cells. For suppression of the molecular photodegradation, we propose to directly remove the excited energy from the DUV-absorptive molecules. This can potentially be very effective in directly reducing photodegradation, since the excited states of the DUV-absorptive molecules are the fundamental origins of the cellular photodegradation [18]. We used terbium, europium, and thulium (Tb^{3+}, Eu^{3+}, and Tm^{3+}), which are trivalent ions in the lanthanide group (Ln), to remove the excited energy of the DUV-absorptive molecules. These were chosen because Tb^{3+} and Eu^{3+} are known as energy quenchers of nucleobases [35–39] and aromatic amino acid [35,40,41], while Tm^{3+} has similar electronic properties [42] to Tb^{3+} and Eu^{3+}. The effects of Ln ions for suppressing the molecular photodegradation were quantified by comparing the effects of DUV light on the morphologies of fixed HeLa cells with and without these ions. The direct measurement of resonant molecules was also evaluated by resonant Raman scattering of nucleobases, which are some of the most DUV-fragile molecules present in the cells [18,19]. The present study, showing suppression of the molecular photodegradation under DUV exposure for the first time, indicates an important first step towards the practical use of DUV imaging in a variety of biological applications.

2. Materials and methods

2.1.Cell culturing, fixation, and permeabilization

HeLa cells were cultured in Dulbecco's Modified Eagle's Medium on a fused silica cover slip for 22-26 hours at 37 degree C in 5% CO_2 atmosphere with 100% RH. The cultured cells were fixed with 4% paraformaldehyde in phosphate buffered saline (PBS) solution for 5 min. The fixed cells were permeabilized with 0.5% Triton-X in PBS solution for 15 minutes.

2.2. Cell treatment with lanthanide ions

For samples treated with Ln ions, the fixed and permeabilized cells were immersed in the buffer solution (pH = 7.4) containing 10 mM HEPES, 4 mM KCl, 1 mM $MgCl_2$, 1 mM $CaCl_2$, 149.4 mM NaCl, 4 mM NaOH, and either of $TbCl_3$, $EuCl_3$, and $TmCl_3$ [43]. Unless noted, the agent concentration was 1 mM. The cells were immersed in the solution for 30 minutes or longer before DUV irradiation and Raman measurement.

For control samples, the fixed and permeabilized cells were immersed in the buffer solution, without containing any of the agents.

$TbCl_3$ and $EuCl_3$ were purchased from Kojundo Chemical Laboratory. $TmCl_3$ was purchased from Sigma-Aldrich.

2.3. Optical measurement

A homebuilt DUV Raman microscope was used for DUV Raman measurement. A light source was Ar^+ laser of $\lambda = 257.2$ nm (Innova, Coherent). The expanded and collimated beam was focused by an NA = 1.35 objective lens (Ultrafluar, Carl Zeiss) at a distance of 2 μm from the substrate surface. The beam was incident from the cover slip side. Sample exposure duration was controlled with a mechanical shutter. Sample irradiation intensity was controlled by ND filters and set to 200 $\mu W/\mu m^2$. The sample was located on a piezoelectric stage. For Raman signal detection from the sample, backscattering light collected with the objective lens was used. The backscattering light passed through an edge-filter (LP02-257RU, Semrock), and entered the spectrometer (SP2500, Acton Research) through an entrance slit (50 μm). A focusing lens situated in front of the slit was adjusted to best guide Raman scattering light into the spectrometer. Raman scattering entering the spectrometer was dispersed with a grating (1800 g/mm). The spectrometer was calibrated with the laser line (0 cm^{-1}), and Raman scattering of BN (1364 cm^{-1}) and CH_3CN (2249 cm^{-1}). The dispersed light was detected with a CCD camera (ProEM, Princeton Instruments) and recorded using WinSpec

#253648 Received 9 Nov 2015; revised 8 Dec 2015; accepted 11 Dec 2015; published 18 Dec 2015

(Princeton Instruments). For imaging, the cells were raster-scanned over a focused DUV light. Shutter operation, stage scan, and camera acquisition were synchronized by a computer installing IGOR Pro. The cells were irradiated only at the dwell time. Scan step was 500 nm. Pixel dwell time was 250 ms unless otherwise noted. The polarization of the laser beam was linear. The laser beam was spatially filtered by a pinhole to make a tight focus with little aberration.

Bright-field images shown in this manuscript were taken before and after DUV Raman imaging. Visible light was used for taking the bright-field images.

Luminescence spectral imaging of Ln ions was also performed. For measurement, a homebuilt DUV-excitation, UV-visible detection spectral imaging system was used. The system basically shared the excitation setup with the DUV Raman microscope, but replaced the NA = 1.35 objective lens by an achromatic objective lens (UV 50xA, Nikon Engineering) for the wide spectral range measurement. Excitation and emission light were separated by a dichroic mirror (FF310-Di01, Semrock). Emission spectra were recorded with a CCD camera (iXon3 888, Andor) using the software of Solis (Andor) through a spectrometer (CLP-105UV, Bunko Keiki) having a 140 μm entrance slit and a 300 g/mm grating. The spectrometer was calibrated with a mercury lamp. The imaging mode was the same as the one used for Raman imaging. Scan step was 500 nm. Pixel dwell time was 50 ms.

2.4. Image data analysis

A spectral data set recorded by a single Raman imaging process was a two-dimensional data (one spatial dimension vs wavenumber). The data was processed for Raman image reconstruction. A macro program constructed in MATLAB was used. First, any anomalously sharp peak in the spectrum, such as cosmic rays, was removed using a median filter. Then, the spectra were smoothed by taking moving average of 5 pixels. Finally, 5th-order polynomial curve fitting with an alternative least square algorithm with 50 iterations was applied to each spectrum and the curve obtained as the fluorescent background was then subtracted from the spectrum. To reconstruct Raman images, the intensity at 1480 cm^{-1} and neighboring ± 3 pixels (a range of ~28 cm^{-1}) was averaged.

Raman signal from the cell's nucleus was analyzed using ImageJ. First, the nucleus area was selected from a cell and the intensity was averaged by area. To remove the influence of background in the results, the intensity at some pixels corresponding to the substrate area was averaged from all the data taken in the same measurement and sample conditions, then the average background intensity was subtracted from the average nucleus intensity of each data.

The image gradient of a bright-field image was calculated on MATLAB. Only the Raman targeted area was used. The image gradient was calculated at each pixel. As each side of the cell will feature positive/negative gradients, the absolute value of the gradient was taken and then summed to provide a simple metric for the presence of cellular morphology.

3. Results

3.1 Lanthanide ion protection of cell morphology under DUV exposure

Figure 1 shows the effect of loading Ln ions, before and after DUV exposure, on the morphologies of the fixed HeLa cells. It is obvious from Figs. 1(a) and 1(e) that the cells without Ln ion suffered complete loss of structure after DUV exposure. Since the cells were fixed, the cells didn't move significantly during scanning (taking around 25 min for a single imaging acquisition). The structural loss could occur due to damage and molecular decomposition at the irradiated regions and its accumulation during scanning. The loss of cellular structure is a typical phenomenon with cellular samples exposed to DUV light for the irradiation parameters used (50 μJ/μm^2) in our experiments. For cells loaded with Tb^{3+}, Eu^{3+}, or Tm^{3+}, the phenomenon of structural loss was not observed; the cellular structures are clearly maintained through DUV exposure while slight shrinkage of the cells occurred (Fig. 1(b)-1(d), and 1(f)-1(h)). The shrinkage mechanism may result from the inability of the lanthanide ions to provide complete protection to all cellular molecules, especially the

#253648 Received 9 Nov 2015; revised 8 Dec 2015; accepted 11 Dec 2015; published 18 Dec 2015

molecules that sustain cellular structure. Alternatively, it may be an independent mechanism. These results are reproducible, despite variations in individual cell states such as cell morphology and molecular distributions. Figure 1(i) shows a histogram representing the morphological changes of irradiated cells. The cellular morphologies are quantified using the gradient of the bright-field image. While a fully quantitative cellular metric using the image gradient would require a quantitative phase imaging mode [44], the image gradient of the bright-field image includes absorption and lensing effects, leading to changes in brightness in regions where cells exist. This provides a simple metric to evaluate the presence of cell morphology. Using the absolute value of the image gradient allows the metric to be positive for any structural feature. The difference in this gradient before and after DUV exposure can then indicate the loss of cell material, while no change means that the cellular morphologies are maintained. Without Ln ion, the summed absolute image gradient values over the irradiated areas consistently decreased with DUV exposure, meaning that all the cells without Ln ion lost a significant amount of cellular structure. Evaluation by eye of the bright-field images also shows near-complete loss of the sample in the area that was exposed. On the other hand, all results using any of Tb^{3+}, Eu^{3+}, and Tm^{3+} show near-zero or positive values. The positive values can be explained by slight shrinkage of the irradiated cells seen in Figs. 1(b)-1(d) and 1(f)-1(h), which in general makes the image gradients larger due to concentration of materials. Inspection of the images reveals the cells remain structurally intact. These results showed that Tb^{3+}, Eu^{3+}, and Tm^{3+} consistently prevented the loss of cellular materials under DUV exposure.

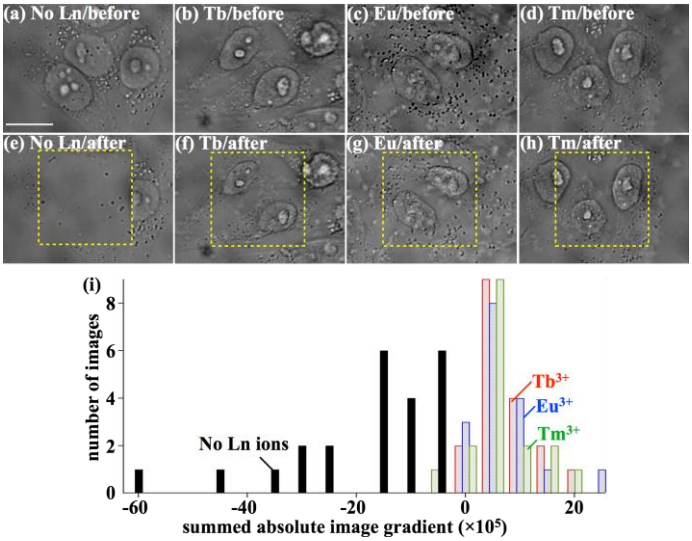

Fig. 1. The addition of Ln ions protects cell morphology from DUV irradiation. (a-h) Bright-field images of the fixed HeLa cells (a-d) before and (e-h) after DUV exposure are shown. The cells shown in (a) and (e) were not treated with Ln ions, while the cells shown in (b) and (f), (e) and (g), and (d) and (h) were treated with Tb^{3+}, Eu^{3+}, and Tm^{3+}, respectively. The scale bar is 15 μm. The dotted squares exhibit the DUV irradiation areas. (i) A histogram for the bright-field images from all data (n = 75) including n = 153 irradiated cells. The distribution of the differences in normalized, summed absolute image gradient between before and after DUV irradiation is shown.

3.2 Lanthanide ion protection nucleobases measured by resonance Raman scattering

The above section shows clearly that the bulk cellular structure is protected by the Ln ion technique, but to further understand whether Ln ions protect individual molecules as well as the bulk structure, we can use Raman scattering to determine how cellular molecules are protected from DUV exposure. Raman scattering excited by DUV light is a sensitive probe of nucleobases in the cell [19,25], due to the resonance Raman effect. Nucleobases are directly

#253648 Received 9 Nov 2015; revised 8 Dec 2015; accepted 11 Dec 2015; published 18 Dec 2015

excited by DUV light and therefore, along with aromatic amino acids [18,19], are some of the most fragile molecules in cells for DUV exposure [18,19]. The use of DUV Raman scattering measurement is then ideal since it should measure the molecules that are most susceptible to photodegradation. Furthermore, the Raman scattering intensity can be used to quantify the effects of Ln ions on the molecular photodegradation by estimating the relative number of undamaged molecules over DUV exposure. Raman intensity images were taken so that each spatially-resolved pixel in the sample contained the measured Raman spectrum (see Materials and Methods for more details). For comparison, images using contrast from the 1480 cm^{-1} band in the spectrum (Fig. 2(a)), which is intense and assigned only to adenine and guanine [25,45], showed that Tb^{3+}, Eu^{3+}, and Tm^{3+} provided higher image contrasts than the control experiment without Ln ion. The higher contrast shows the cellular nuclei and nucleoli, where nucleic acids exist at high concentrations, and the cytoplasm, in which a number of RNAs are distributed (Figs. 2(b)-2(e)). In addition, it is apparent that Raman signal levels measured from the cells loaded with Tb^{3+}, Eu^{3+}, and Tm^{3+} are higher than the control (in Fig. 2(b)-2(d) vs Fig. 2(e)). These results prove that Ln ions can protect the DUV-excited, most fragile molecules in the cells under DUV exposure.

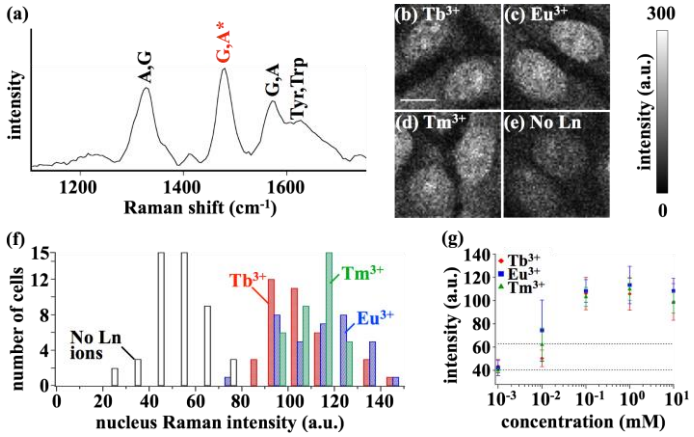

Fig. 2. Protecting effect of Ln ions measured by Raman scattering. (a) A typical DUV Raman spectrum obtained from the cell; A: adenine, G: guanine, Tyr: tyrosine, Trp: tryptophan. The asterisk indicates the Raman band used for reconstructing Raman intensity images. (b-e) Raman intensity images reconstructed by the nucleobases band of the cells treated with (b) Tb^{3+}, (c) Eu^{3+}, or (d) Tm^{3+}, and (e) without Ln ion. The scale bar is 10 μm. (f) A histogram for the average Raman intensity in the nuclei for a number of the measured cells, with or without Tb^{3+}, Eu^{3+}, and Tm^{3+}. The number of cells analyzed is 47, 36, 35, and 35, for no Ln ion, Tb^{3+} Eu^{3+}, and Tm^{3+}, respectively. (g) Concentration dependencies of the nuclei Raman intensity for Tb^{3+}, Eu^{3+}, and Tm^{3+}. The plots, and the positive/negative error bars show the average Raman intensity and standard deviations of a number of cells. The upper, and lower horizontal dotted line represents the average Raman intensity plus, and minus standard deviation for no Ln ion, respectively. The number of analyzed cells is 10 for 1 μM Tb^{3+} and Eu^{3+}, 11 for 1 μM Tm^{3+}, 20 for 10 μM Tb^{3+} and Eu^{3+}, 100 μM Tb^{3+}, Eu^{3+}, and Tm^{3+}, and 10 mM Tb^{3+} and Eu^{3+}, 21 for 10 μM and 10 mM Tm^{3+}, 35 for 1 mM Eu^{3+} and Tm^{3+}, 36 for 1 mM Tb^{3+}, and 47 for no Ln ion, respectively.

To quantify the increase in Raman signal levels under Ln ion treatment, all the measured Raman images of the cells (n = 106 cells with Ln ions, n = 47 cells without Ln ion) were quantitatively analyzed. The Raman intensity of the nucleus was analyzed, since the nucleus provided a sufficiently high SNR for an accurate Raman intensity analysis. The results are summarized in Fig. 2(f) as a histogram. Despite individual cell variations, the Raman signal of all the cells treated with any of the three Ln ions, excluding only one cell out of n = 106 cells, is larger than that of the cells without Ln ion. The maximum difference in Raman signals due to the loading of Ln ions is six times higher and on average, the Raman signal indicates approximately twice as many nucleobases could provide Raman scattering before photodegradation occurred under DUV exposure. Additionally, the three different Ln ions

#253648 Received 9 Nov 2015; revised 8 Dec 2015; accepted 11 Dec 2015; published 18 Dec 2015

showed little difference between them in measured nuclei Raman intensity. All three appeared similar in the histogram (Fig. 2(f)), as did the averages and standard deviations of the Raman intensities (shown in Fig. 2(g)), indicating that they play a similar role for protecting nucleobases from DUV irradiation.

We confirmed that the Raman measurement of the protection effect above was not influenced by any enhancement of the scattering efficiencies of adenine and guanine due to interactions with Ln ions. We measured adenine and guanine in water with and without Ln ions (Fig. 3). Here, due to diffusion, any molecular photodegradation during DUV Raman measurement should not significantly affect the signal levels, and therefore Raman signals with or without Ln ions are expected to be similar if no enhancement by Ln ions occurs. The results in this configuration with and without Ln ions indeed do not show any clear differences. Thus, we concluded that the Raman signal increase by the Ln ions in the cell measurements results from suppression of the molecular photodegradation by the Ln ions.

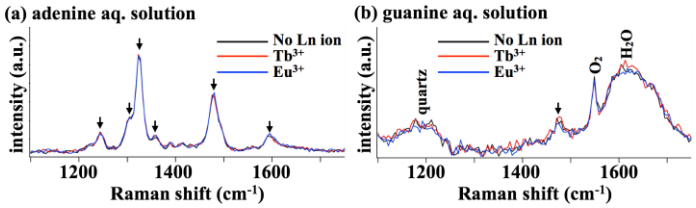

Fig. 3. DUV resonance Raman spectra of the (a) adenine and (b) guanine aqueous solutions. Arrows indicate the Raman bands assigned to adenine or guanine. In (a), Raman spectra of the 1 mM adenine aqueous solutions with and without Tb^{3+} or Eu^{3+} are shown together. In (b), Raman spectra of the saturated guanine aqueous solutions with and without Tb^{3+} or Eu^{3+} are shown together.

Raman scattering measurements also revealed that suppression of the molecular photodegradation under DUV exposure could depend on the concentration of Ln ions. Although it is not trivial to separate concentration dependencies from other parameters such as exposure duration and irradiation intensity, if the experimental parameters are fixed for a given condition, then the optimal concentration for effectively suppressing the nucleobases photodegradation can be found for that condition. The Raman nuclei intensity of cells treated with Tb^{3+}, Eu^{3+}, or Tm^{3+} at different concentrations is shown in Fig. 2(g). The results show that all three Ln ions exhibit similar concentration dependencies. 100 μM and 1 mM provided higher Raman signals due to effective photodegradation suppression than other concentrations. 1 μM was found to be too low to suppress the photodegradation. Interestingly, 10 mM exhibits a slight decrease in the signal compared to 1 mM. One possible reason for this decrease could be related to a pH drop in the solution caused by Ln ions addition; while a pH drop was measured at only 0.05 for 1 mM, it did rise to 0.3 at 10 mM. Such a pH change of 0.3 would be large enough for the electronic states of Eu^{3+} and Tb^{3+} to be altered [46], implying that energy transfer efficiency may be modified by a 0.3 pH change. To elucidate the underlying science, further studies with varying measurement parameters such as exposure duration, irradiation intensity, and solution pH, would be necessary.

3.3 Enabling repetitive deep-UV imaging by lanthanide ion nucleobase protection

The photodegradation suppression could improve the SNR of the images taken using DUV resonance Raman scattering, as shown in Fig. 2. The protection of the molecules also allowed repeated measurements in DUV resonance Raman cellular imaging, which was not otherwise possible (Fig. 4). The effect of Ln ions was clearly visible after the first Raman imaging. Without Ln ion, the second image (Fig. 4(a)) displayed only vague outlines of the nucleus, and the third image (Fig. 4(c)) showed only noise, whereas with Ln ions, clear nuclei and cytoplasmic structures were retained in the second (Fig. 4(e)) and third (Fig. 4(f)) imaging. The cells with Ln ions remained in place after the third imaging (Figs. 4(i) and 4(j)), while the cells without Ln ion disappeared (Figs. 4(g) and 4(h)). Raman spectra acquired from the cell

#253648 Received 9 Nov 2015; revised 8 Dec 2015; accepted 11 Dec 2015; published 18 Dec 2015

also clearly present the protective effect of Ln ions on repetitive DUV measurement of the cells (Figs. 4(k) and 4(l)). Four observable Raman bands, that are assigned to nucleobases (1340, 1480, and 1580 cm^{-1}) [25,45] or aromatic amino acids (1620 cm^{-1}) [25,45], were barely observed in the results obtained during the second and third imaging measurements of the cell without Ln ions (Fig. 4(k)), while with Ln ions (Fig. 4(l)), these bands were observable through three-time repetitive imaging.

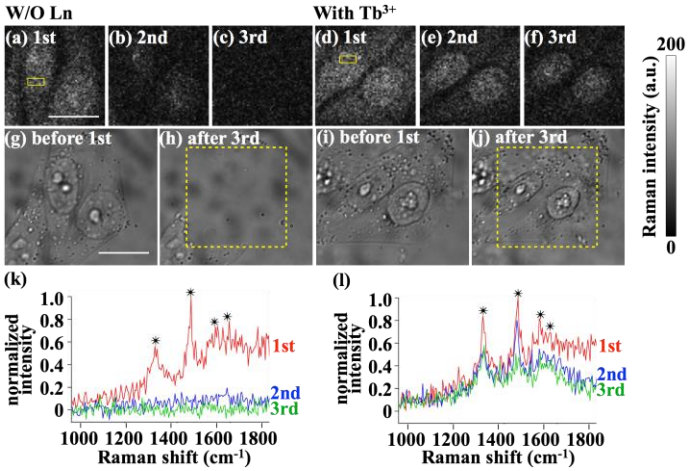

Fig. 4. Repetitive measurements on fixed HeLa cells by DUV Raman imaging. (a-f) Raman intensity images repeatedly measured from identical cells treated (a-c) without Ln ion and (d-f) with Tb^{3+}. (a) and (d) were measured at first, and (c) and (f) were measured at the end. The exposure duration for acquiring a single-point spectrum was 100 ms. (g-j) Bright-field images of the cells measured (g and i) before the 1st Raman imaging, and (h and j) after the 3rd Raman imaging. The cells shown in (i) and (j) were treated with Tb^{3+}, while the cells in (g) and (h) were not. The dotted squares depict the DUV irradiation areas. The scale bars are 15 μm. (k,l) Average Raman spectra obtained for each imaging acquisition from the cell nucleoplasm region discriminated by the yellow solid square in (a), and (d) are shown in (k), and (l), respectively. The asterisks indicate the observable Raman bands of nucleobases or aromatic amino acids. Red, blue, and green spectra represent the results of 1st, 2nd, and 3rd imaging acquisition, respectively. The presented spectra were processed for display; the bias was removed first by subtracting the average intensity of noise obtained from region outside the cells, and then the spectra in (k) and (l) were normalized by the peak intensity of the 1480 cm^{-1} band of each "1st" spectrum.

4. Discussion

The fundamental origin of nearly all the molecular photodegradation discussed here involves electronic excited states of nucleobases and aromatic amino acids. This is because other molecules in the cell have relatively low absorption at these DUV wavelengths (λ = 257 nm) [18,19]. A summary of the energy pathways of the DUV-excited molecules in the cells under DUV exposure is shown in Fig. 5. Without Ln ion (Fig. 5(a)), nucleobases and aromatic amino acids can be ionized [12–15,18,20,21]. Reaction with surrounding molecules such as nucleobases, aromatic amino acids, and O_2 can also occur, resulting in irreversible formation of photoproducts (i.e. cyclobutane pyrimidine dimer, 2,2'-bityrosyl, and 8-oxo-7,8-dihydro-2'-deoxyguanosine) [12-15,18.20,21]. Relaxation of excited nucleobases and aromatic amino acid can also occur, without causing the molecular photodegradation, through thermal and radiative decays [21,47–49]. However, the remainder of the energy can thereby transfer to surrounding molecules, including O_2, resulting in ionization [18] and reactions with surrounding molecules [12,13,15,18,20,21], including generation of ROS, which can modify molecules that would otherwise be transparent to DUV light [18].

Possible energy pathways of the DUV-excited molecules in cells treated with Ln ions are shown in Fig. 5(b). We predicted an additional relaxation pathway due to Ln ions by

#253648 Received 9 Nov 2015; revised 8 Dec 2015; accepted 11 Dec 2015; published 18 Dec 2015

considering Förster resonance energy transfer (FRET). Tb^{3+} and Eu^{3+} have been reported to quench the DUV-excited states of nucleobases [35–39] and aromatic amino acids [35,40,41] through FRET. Although Tm^{3+} has not been reported to act as an energy quencher of nucleobases and aromatic amino acids, we expected Tm^{3+} could work similarly to Tb^{3+} and Eu^{3+} because Tm^{3+}, Tb^{3+}, and Eu^{3+} are used in similar applications that rely on their emissive properties after conjugation to materials [42]. If energy quenching occurs, it can suppress the

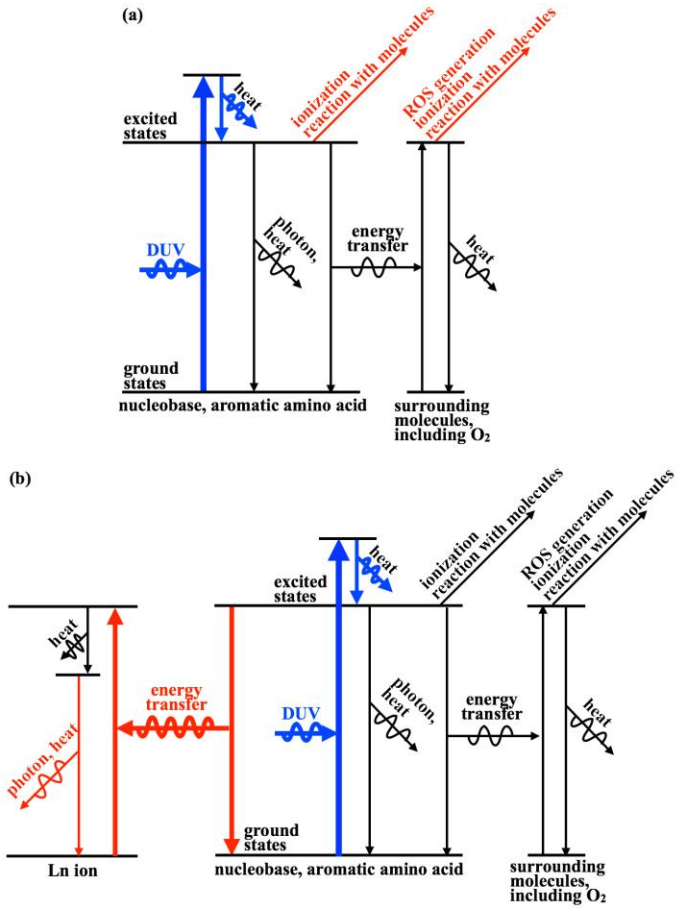

Fig. 5. Energy pathways of nucleobases and aromatic amino acids in a cell under DUV (λ = 257 nm) exposure. Regardless of the type of Ln ion, nucleobases or aromatic amino acids are excited by absorbing DUV light, then is immediately relaxed to the vibrational ground state of the electronic excited state having the lowest energy. (a) Without Ln ion, the excitation of nucleobase or aromatic amino acid is followed by ionization, reaction with molecules, and relaxation to the electronic ground state. The relaxation pathways are thermal and radiative decays or energy transfer to surrounding molecules. The energy transfer to surrounding molecule is followed by ROS generation, ionization, reaction with molecules, and thermal decay. (b) With Ln ion, FRET from the excited nucleobase and aromatic amino acid to the higher energy level of Ln ion can occur. Ln ion is relaxed to the lower excited energy states by heat emission and further relaxed by thermal or radiative decays.

molecular photodegradation through any pathway except for heat-based pathways; energy quenching can accelerate relaxation of the excited state of a donor molecule, and thereby Ln ions can suppress the ionization and reaction of the DUV-excited molecules. Additionally, energy transfer to Ln ions can suppress energy transfer to surrounding molecules and ROS generation, and consequently protect surrounding molecules. The contribution of these

#253648 Received 9 Nov 2015; revised 8 Dec 2015; accepted 11 Dec 2015; published 18 Dec 2015

mechanisms in suppressing the photodegradation can be large when the efficiency of the energy transfer to Ln ions is comparable to or higher than that for transfer to O_2. Although quantum yields for energy transfer from nucleobases, and aromatic amino acids to the three Ln ions and to O_2 are poorly understood, one report in the literature [41] states the quantum yield of the energy transfer from tryptophan to Eu^{3+} was 50%. This relatively high value for the yield must exceed the efficiency of energy transfer from tryptophan to O_2, and can support the above-mentioned mechanisms for Ln ions suppression of cellular photodegradation.

The removal of energy by heat or photon emission from Ln ion was also considered in the mechanisms. We confirmed Tb^{3+} could emit light in the cells under DUV (λ = 257 nm) exposure, by performing luminescence spectral imaging of the cells treated with Ln ions (Fig. 6). Results indicate that Tb^{3+} can emit energy by radiative decay after accepting the energy from the excited molecules. In fact, with DUV excitation, Tb^{3+} is reported to emit light, when conjugated to a protein [35,41]. On the other hand, we found Eu^{3+} and Tm^{3+} could not emit light in the cells under DUV (λ = 257 nm) exposure, although Eu^{3+} and Tm^{3+} are known as emissive ions in general [42]. According to literature, Eu^{3+} under DUV excitation doesn't emit light [35,41] and thermally decays [35]. Based on the fact that Eu^{3+} does, we expect Tm^{3+} to also decay by a thermal process.

The measured dependencies of the protection effects on the Ln ions concentration (Fig. 2(g)) can partially support the predicted mechanism of the protection effect. According to literature, FRET from Ln ion to nucleobase can occur when the concentration of Ln ions is 0.1 mM or less [37,38], consistent with the results shown in the Fig. 2(g). Provided that the parameters such as pH could be maintained while changing the Ln ions concentration, significantly higher concentration could possibly provide higher protection effect because of the presumably higher FRET efficiency. Indeed, the donor-acceptor distance for the FRET efficiency to be 50% is generally in the range of 2-50 mM [50], predicting the higher protection effect at the higher concentration.

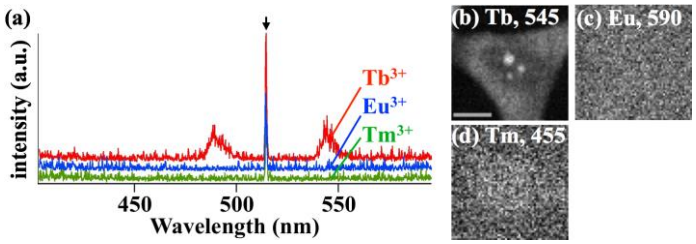

Fig. 6. (a) DUV-excited luminescence of nuclei of cells treated with Tb^{3+}, Eu^{3+}, or Tm^{3+}. (b-d) Luminescence intensity distribution of cells treated with (b) Tb^{3+}, (c) Eu^{3+}, and (d) Tm^{3+}. (b) was reconstructed by the luminescence band at λ = 545 nm, while (c), and (d) were reconstructed at λ = 590, and 455 nm, where Eu^{3+}, and Tm^{3+}, when excited with proper wavelengths, should have an emission line, respectively[35,42]. The scale bar is 10 μm. The arrow indicates the second-order diffraction light of the laser line (λ = 257 nm), at λ = 514 nm.

5. Future perspectives

We demonstrated Ln ion molecular protection, and showed that it enables the use of DUV molecular imaging which would otherwise not be possible. However, the effect does still have limits, and further improvement would still be of interest. By evaluating ROS effects, we found that some of the excited energy was still transferred to O_2, causing O_2-based damage to the cells (Fig. 7 and Table 1). Possible energy pathways to O_2 can be derived not only from the DUV-excited molecules but also from the quenching Ln ions that accept energy from the DUV-excited molecules. Such energy retransfer from Ln ion to O_2 is possible because the lifetimes of Tb^{3+} and Eu^{3+} (which are of millisecond order [35]) are much longer than that of typical fluorescent molecules (of nanosecond order [51]) that are known to readily transfer energy to O_2 for ROS generation [51]. Improving the efficiencies of energy transfer from DUV-excited molecules to Ln ions and the energy emission from Ln ions,

#253648 Received 9 Nov 2015; revised 8 Dec 2015; accepted 11 Dec 2015; published 18 Dec 2015

which can suppress the remaining energy pathways to O_2, will be critical future considerations arising from this study. Importantly, since the protection mechanism should be universal, this research should not be limited to use of Ln ions but should be extensible to exploration and/or development of new materials that have high efficiencies of energy transfer from DUV-excited molecules.

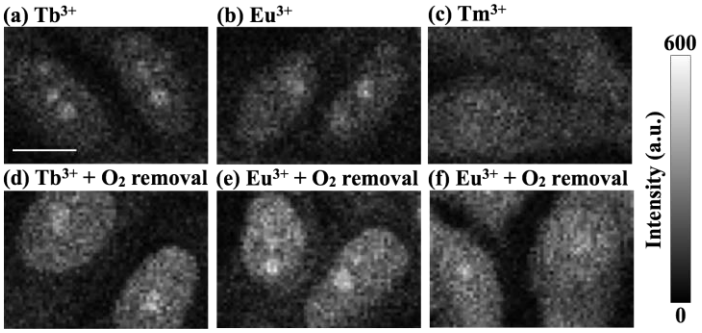

Fig. 7. Ln ion molecular protection under (a-c) the standard ambient and (d-f) the low-O_2 conditions. The cells treated with (a) Tb^{3+}, (b) Eu^{3+}, and (c) Tm^{3+}, in the standard ambient condition, exhibit weaker Raman signals compared to the cells treated with (d) Tb^{3+}, (e) Eu^{3+}, and (f) Tm^{3+}, in the low-O_2 condition, respectively. The scale bar is 10 μm. The exposure duration for a single Raman spectrum acquisition was 500 ms. O_2 in the sample environment was removed by using the Ar purge process. For the Ar purge process, a glove box chamber was used. After the fixed and permeabilized cells were put inside the chamber, the O_2 level inside the chamber was decreased by Ar input and air output. The chamber was then sealed and left for 20 min while keeping the O_2 level lower than 2.0%. Finally, the cells were sealed. Ar gas was purchased from Awao-Sangyo.

Table 1. Averages and standard deviations of the nuclei Raman intensity of cells treated with Tb^{3+}, Eu^{3+}, and Tm^{3+} under the standard ambient and the low-O_2 conditions.

Conditions	Average	Standard deviation	Number of cells
Tb^{3+}	123.3	17.5	10
Tb^{3+} & O_2 removal	146.0	25.6	10
Eu^{3+}	116.1	22.7	10
Eu^{3+} & O_2 removal	193.4	15.1	11
Tm^{3+}	124.1	16.6	11
Tm^{3+} & O_2 removal	172.3	16.4	11

Application to biological protection from DUV light is also of significant interest. The presented mechanisms for protecting molecules will not be limited to molecular protection under DUV exposure. The retention of the cell shape under DUV irradiation implies that this technique may be applied to living organisms. For living specimens, however, membrane permeability is essential, where Ln ions can be loaded inside the cells requiring membrane permeabilization pretreatment. The biocompatibility of the compounds also needs to be considered. For improvement of the protection efficiency in living specimens, a method that only minimally affects sample homeostasis will be preferable. Other future directions of the presented work include extension to other spectral ranges. Energy manipulation and emission of the excited molecules can occur and may work also in other wavelength ranges, for protecting excited and surrounding molecules. A range of optical techniques that are currently limited in application by specimen photodegradation could undergo significant breakthroughs by extension of the methods in the present study.

#253648 Received 9 Nov 2015; revised 8 Dec 2015; accepted 11 Dec 2015; published 18 Dec 2015

Acknowledgments

This work was financially supported by JSPS Grant-in-Aid for Young Scientists (B) 25871127 and for Scientific Research (S) 21226003. The authors sincerely acknowledge Dr. A. Taguchi of Osaka Univ., Dr. K. Furusawa of NICT, and Dr. J. Ando of RIKEN for valuable suggestions and discussions, Dr. A. F. Palonpon of Osaka Univ. for Raman image reconstruction, and PARC at Osaka Univ. for sharing laboratory apparatus.

#253648 Received 9 Nov 2015; revised 8 Dec 2015; accepted 11 Dec 2015; published 18 Dec 2015